Geochemistry, Geophysics, Geosystems®

AGU ADVANCING EARTH AND SPACE SCIENCE

RESEARCH ARTICLE
10.1029/2022GC010621

Key Points:

- New P-wave tomographic model highlights mid- and lower mantle structure beneath Africa
- Volcanism in Cameroon is linked to the Large Low Velocity Province beneath southern Africa
- Models that relate Cameroon volcanism solely to edge-driven flow are inconsistent with the presented findings

Supporting Information:

Supporting Information may be found in the online version of this article.

Correspondence to:

H. Saeidi,
hsaeidi@crimson.ua.edu

Citation:

Saeidi, H., Hansen, S. E., & Nyblade, A. A. (2023). Deep mantle influence on the Cameroon Volcanic Line. *Geochemistry, Geophysics, Geosystems*, *24*, e2022GC010621. https://doi.org/10.1029/2022GC010621

Received 14 JUL 2022
Accepted 15 DEC 2022

Author Contributions:

Conceptualization: Samantha E. Hansen, Andrew A. Nyblade
Data curation: Hesam Saeidi, Samantha E. Hansen
Formal analysis: Hesam Saeidi, Samantha E. Hansen
Funding acquisition: Samantha E. Hansen
Investigation: Hesam Saeidi, Samantha E. Hansen, Andrew A. Nyblade
Methodology: Hesam Saeidi, Samantha E. Hansen
Project Administration: Samantha E. Hansen, Andrew A. Nyblade
Resources: Hesam Saeidi, Samantha E. Hansen, Andrew A. Nyblade

Deep Mantle Influence on the Cameroon Volcanic Line

Hesam Saeidi[1], Samantha E. Hansen[1], and Andrew A. Nyblade[2]

[1]Geological Sciences Department, The University of Alabama, Tuscaloosa, AL, USA, [2]Geosciences Department, The Pennsylvania State University, University Park, PA, USA

Abstract The origin of the Cameroon Volcanic Line (CVL), which is difficult to explain with traditional plate tectonics and mantle convection models because the volcanism does not display clear age progression, remains widely debated. Existing seismic tomography models show anomalously slow structure beneath the CVL, which some have interpreted to reflect upper mantle convective processes, possibly associated with edge-driven flow related to the neighboring Congo Craton. However, mid- and lower mantle depths are generally not well resolved in these models, making it difficult to determine the extent of the anomalous CVL structure. Here, we present a new P-wave velocity model for the African mantle, developed with the largest collection of travel-time residuals recorded across the continent to date and an adaptive model parameterization. Our extensive data set and inversion method yield high resolution images of the mantle structure beneath western Africa, particularly at the critical mid- and lower mantle depths needed to further evaluate processes associated with the formation of the CVL. Our new model provides strong evidence for a connection between the African Large Low Velocity Province, centered in the lower mantle beneath southern Africa, and the continental portion of the CVL. We suggest that seismically slow material generated near the core-mantle boundary beneath southern Africa moves northwestward under the Congo Craton. At the northern edge of the craton, the hot, buoyant material rises through the upper mantle, causing the CVL volcanism. Consequently, CVL magmatism can be linked to large-scale mantle processes rooted in the deep mantle.

Plain Language Summary Similar to the Hawaiian island chain, the Cameroon Volcanic Line (CVL) is comprised of a linear series of volcanic centers; however, the CVL does not display the same type of age progression as that seen in Hawaii. As such, it is difficult to explain the CVL with traditional plate tectonic and hotspot models, leaving the CVL origin open for debate. Using the travel-times of earthquake signals recorded by stations in Africa, along with a modeling approach that is based on the data sampling density, we have developed a new model that reveals the seismic velocity structure beneath the CVL throughout the mantle. Compared to previous seismic models, our results provide improved imaging of structural characteristics at mid- and lower mantle depths, thereby allowing us to reevaluate CVL origin models. Our results indicate that hot material generated near the core-mantle boundary beneath southern Africa flows northwestward beneath the Congo Craton. When this hot, buoyant material reaches the northern edge of the craton, it rises through the mantle and ultimately provides the source of volcanic activity within the CVL. These findings emphasize that large-scale mantle flow can have significant impacts not only on deep Earth structure but also at the surface.

1. Introduction

The 1,600-km long Cameroon Volcanic Line (CVL), which extends from Lake Chad to the western coast of Africa and continues offshore into the Atlantic Ocean (Figure 1a), is marked by intraplate, mafic alkali volcanic centers (Déruelle et al., 1991; Fitton & Dunlop, 1985; Meyers et al., 1998; Moreau et al., 1987; Poudjom Djomani et al., 1997). This linear volcanic chain does not display age progression (especially the onshore segment), and as such, it is challenging to explain within the traditional plate tectonic paradigm. Linear volcanic chains like the CVL (Bonneville et al., 2006; Koppers et al., 2003; McNutt et al., 1997; Sandwell et al., 1995) lack many of the defining characteristics of other volcanic chains explained by lithospheric plates moving over mantle plumes and thus appear to represent an entirely separate mechanism of mantle circulation.

Despite many geophysical and geochemical investigations over the past several decades (see review by Adams (2022) and references therein), the origin of the CVL is still widely debated. Early studies (Burke, 2001; Ebinger & Sleep, 1998; Morgan, 1981) suggested the CVL is associated with a mantle plume or that hot mantle material from eastern Africa may be channelized by thin lithosphere across central Africa. However, neither of these mechanisms explain the lack of volcanic age progression (Fitton & Dunlop, 1985; Halliday et al., 1988)

Software: Hesam Saeidi, Samantha E. Hansen
Supervision: Samantha E. Hansen, Andrew A. Nyblade
Validation: Hesam Saeidi, Samantha E. Hansen
Visualization: Hesam Saeidi, Samantha E. Hansen
Writing – original draft: Hesam Saeidi, Samantha E. Hansen, Andrew A. Nyblade
Writing – review & editing: Hesam Saeidi, Samantha E. Hansen, Andrew A. Nyblade

nor the low CVL eruption rate (Suh et al., 2003). Other studies attribute the CVL to convective flow in the upper mantle; however, even amongst such studies, there is disagreement regarding the driving forces and the convection cell size. For example, Meyers et al. (1998) suggested the CVL results from cylindrical convection cells driven by shear heating across the 660 km mantle discontinuity. Reusch et al. (2010, 2011), Koch et al. (2012), and Adams et al. (2015) instead proposed that convection beneath the CVL is restricted to the upper ~400 km of the mantle, consistent with edge-driven flow (e.g., King, 2007; King & Ritsema, 2000), where lateral temperature differences between the cold, Archean lithosphere of the Congo Craton (Figure 1a) and the thinner, adjacent Proterozoic lithosphere drive small-scale convection. Alternatively, it has been suggested that the CVL may be linked to a deep mantle source. For example, Forte et al. (2010) suggested that hot, buoyant material originating in the deep mantle beneath western Africa separates as it rises into the upper mantle, creating a focused upwelling beneath the CVL. Several global tomographic models (e.g., French & Romanowicz, 2014; Simmons et al., 2010, 2012; Tesoniero et al., 2015) instead provide some indication that the CVL could be associated with the Large Low Velocity Province (LLVP) centered in the lower mantle beneath southern Africa (see Figure S1 in Supporting Information S1), but no prior study has investigated this possibility.

The lack of consensus regarding the CVL origin is partially due to limited seismic constraints on mantle structure. While many tomographic models have been used to investigate the geodynamic processes shaping the African continent (e.g., Bastow et al., 2008; Boyce et al., 2021; Emry et al., 2019; Hansen et al., 2012), most of these models are focused on the East African Rift System and the African LLVP. In western Africa, sparse seismic station coverage (Figure 1b) only allows regional tomographic models to resolve mantle structure above ~500 km depth (Adams et al., 2015; Goussi Ngalamo et al., 2018; Guidarelli & Aoudia, 2016; Reusch et al., 2010), and broader scale models (e.g., Hosseini et al., 2020; Li et al., 2008; Montelli et al., 2004; Zhao et al., 2013) generally have limited resolution (~1,000 km) in the mid- and lower mantle. Therefore, it is difficult to determine the depth extent of the anomalous CVL structure and how it may be connected to larger scale mantle processes.

To further investigate the origin of the CVL, we have developed a new P-wave tomographic model using adaptive parameterization (Hansen et al., 2012; Li et al., 2008) and an expanded travel-time data set (Figure 1b). Our model provides improved resolution at critical mid- and lower mantle depths compared to previous models, particularly for western Africa. We demonstrate that the seismically slow structure imaged beneath the CVL by several previous studies (Adams et al., 2015; Emry et al., 2019; Guidarelli & Aoudia, 2016; Reusch et al., 2010) extends into the deep mantle and is likely connected to anomalous lower mantle structure beneath southern Africa, indicating that the CVL origin is linked to the African LLVP and hence to lower mantle processes.

2. Data and Methodology

2.1. Seismic Data

Much of the data used in our new tomographic model were provided by the International Seismological Center (ISC) catalog, which includes travel-time residuals from local, regional, and teleseismic events. The version of the catalog used in this study contains more than 30 million travel-time residuals from over 550,000 earthquakes that occurred between 1964 and 2016 (Engdahl et al., 1998; Weston et al., 2018). A wide range of P phases is included in the ISC catalog (e.g., P, pP, Pg, Pn, and PKP), which helps to improve the sampling of the Earth's interior structure. However, data recorded by temporary African seismic networks are not included in the global catalog, and for some seismic stations, additional data have become available following the catalog end date. Therefore, we augment the ISC data set with P-wave travel-time residuals from these additional sources. In total, the augmented data set includes data from 1,576 stations in 60 different networks (Figure 1b; see Table 1 for a list of all networks).

To prevent interference from unwanted seismic phases, earthquakes in the augmented data set were limited to epicentral distances of 30–90°, and a minimum moment magnitude (M_W) of 6.0 was required to ensure high signal-to-noise ratio events. Previous studies have highlighted the benefits that waveform alignment and stacking can provide when identifying the arrival times of seismic phases, thereby leading to more robust travel-time residuals (e.g., Boyce et al., 2017; Hansen et al., 2020; Pavlis & Vernon, 2010); therefore, P-wave arrival times for our augmented data set were determined using an iterative, weighted stacking and cross-correlation scheme, which is described in detail in Text S1 of Supporting Information S1. The travel-time residuals for each event-station pair were computed by subtracting the observed arrival time obtained with our correlation approach from that predicted

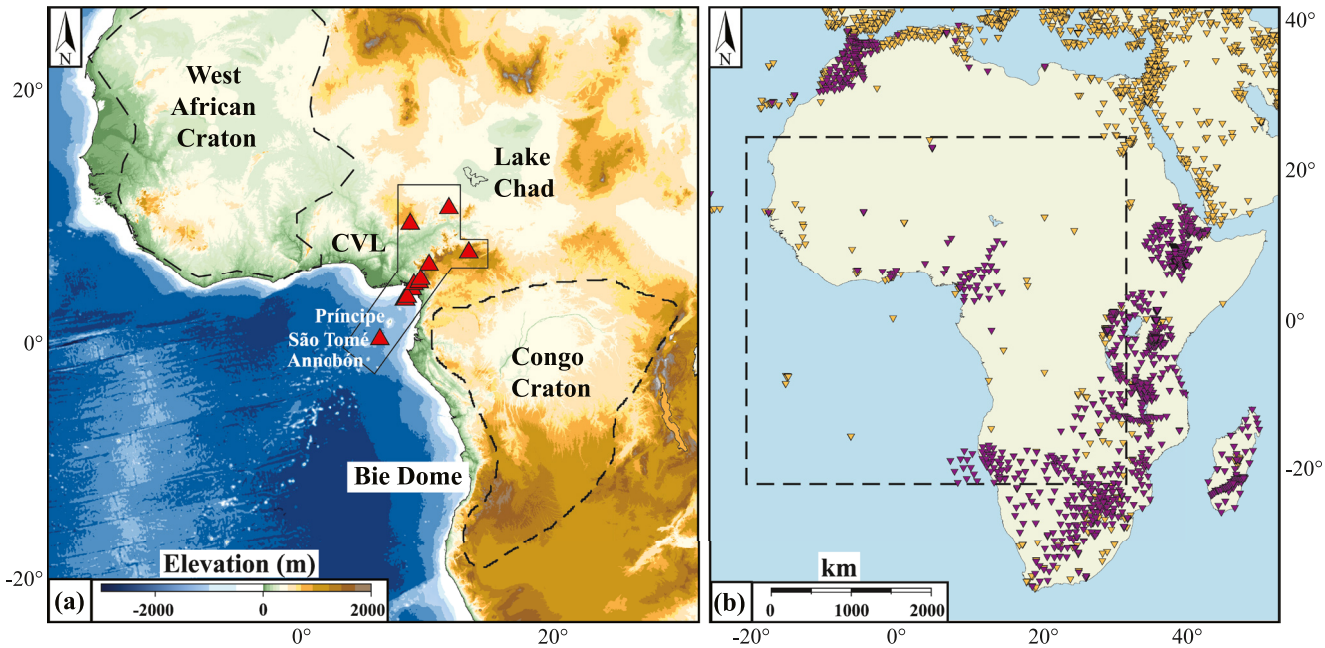

Figure 1. (a) Topographic map of western Africa, showing the juxtaposition of the West African Craton, the Cameroon Volcanic Line (CVL), and the Congo Craton. The locations of Lake Chad and Bie Dome are also indicated. Craton boundaries are denoted with black dashed lines (modified from Emry et al. (2019)), and the Y-shaped feature in the center of the map denotes the surface expression of the CVL. Red triangles indicate the locations of Quaternary volcanoes reported by the Global Volcanism Program (Smithsonian Institution, 2013). (b) Map of Africa showing the distribution of seismic stations used in this study. Orange triangles denote stations that are part of the global International Seismological Center catalog, and purple triangles denote augmented stations. The dashed square indicates the location of the map shown in (a).

by the AK135 model (Kennett et al., 1995). Collectively, the African stations used to create the augmented data set provided more than 102,000 P-wave travel-time residuals that are not included in the ISC catalog.

2.2. Adaptively Parameterized Tomography

The inversion of teleseismic body wave travel-times is a common seismic analysis tool for Earth imaging; however, the nonuniform distribution of seismic stations, combined with the uneven distribution of earthquakes, prevents uniform sampling of the Earth's interior. Despite this, most traditional tomographic methods use a regularly spaced grid to parameterize the model space. As a result, areas with poor seismic ray coverage tend to be over-parameterized, and areas with dense ray coverage lose resolution due to averaging. To overcome these issues, we instead use a tomographic approach where the model gridding is adapted to variations in data coverage (e.g., Kárason & van der Hilst, 2000; Li et al., 2008). Seismic rays between sources and receivers are traced through an initial, regularly spaced grid (~0.7° in latitude and longitude, 45 km in depth), and the number of rays passing through each cell is determined. If the ray count is less than a specified threshold (900), the initial cell is merged with neighboring cells until the minimum ray count is obtained (Figure 2). Ultimately, larger grid cells are developed for poorly sampled portions of the model, while smaller grid cells, allowing for finer resolution, are created in regions with dense data coverage. For our model, the total number of adaptive grid cells is ~763,000, and examples of the adaptive gridding are shown in Figure 2.

The combined ISC and African travel-time residual data set, along with the adaptively parameterized model grid, are employed in an iterative damped least squares approach (Nolet, 1985; Paige & Saunders, 1982) to invert for a global model of the mantle structure. The higher quality African data are given two times the weight in our inversion to balance this data set against the larger but somewhat noisier global data set. As described by Kárason and van der Hilst (2000) and by Li et al. (2008), the misfit function (ϵ), defined by Equation 1 below, is minimized by the inversion process to find the best-fit between the measured travel-time residuals and those predicted by the model.

$$\in = \|\mathrm{Am} - \mathrm{d}\|^2 + k_1\|\mathrm{Lm}\|^2 + k_2\|m\|^2 + k_3\|C - M_c\|^2 \quad (1)$$

Table 1
Seismic Networks Included in Our Augmented Data Set

Network code	Network name/description	Number of stations	Operational duration
1B	Uganda project, JWG University Frankfurt, Germany	30	2006–2008
1C	Seismic Characterization of Menengai Crater, Kenya	23	2011–2014
2H	AFAR0911	23	2009–2013
3D	MOROCCO Network, University Muenster, Morocco	15	2010–2013
5H	Eritrea Seismic Project	7	2011–2012
6A	WALPASS Network, Namibia	41	2010–2012
6H	Mozambique Rift Tomography	28	2011–2013
7C	Yemen Ethiopia Eritrea 2009, DORA Afar temporary experiment	27	2009–2012
8A	AfricaArray—Namibia	19	2015–2018
AF	South Africa National Seismograph Network	49	1980–Present
BX	Botswana Seismological Network	21	2001–Present
DZ	Algerian National Seismic Network	1	2008–Present
G	French Global Network of Seismological Broadband Stations (GEOSCOPE)	5	1982–Present
GE	GEOFON Program, GRZ Potsdam, Germany	11	1995–Present
GH	Ghana Digital Seismic Network	6	2010–Present
GT	Global Telemetered Seismograph Network (USAF/USGS)	4	1993–Present
IB	IberArray	42	2007–2015
II	Global Seismograph Network—IRIS/IDA	3	1990–Present
IU	Global Seismograph Network—IRIS/USGS (GSN)	9	1988–Present
MN	Mediterranean Very Broadband Seismographic Network	5	1988–Present
NJ	Nigerian National Network of Seismographic Stations (NNNSS)	5	2009–Present
NR	Network of Autonomously Recording Seismographs (NARS)	21	1983–Present
TT	Tunisia Broadband Network (TT_Net)	3	2010–Present
WM	Western Mediterranean Seismic Network (WM-Net)	3	2007–Present
XA	Anatomy of an Archean Craton, South Africa, A Multidisciplinary Experiment across the Kaapvaal Craton	82	1997–1999
XB	Broadband Seismic Investigation of the Cameroon Volcanic Line	32	2005–2007
XB	Program to Investigate Convective Alboran Sea System Overturn (PICASSO)	44	2009–2013
XC	Namibia Temporary GEOFON Network	5	1998–1999
XD	Seismic investigations of the Lithospheric Structure of the Tanzanian Craton	21	1994–1995
XI	Seismic Investigation of Deep Structure beneath the Ethiopian Plateau and Afar Depression	38	2000–2002
XJ	Ethiopian Afar Geophysical Lithospheric Experiment	55	2002–2003
XJ	Magadi-Natron Magmatic Rifting Studies	39	2013–2015
XK	Seismic Arrays for African Rift Initiation	53	2012–2014
XM	Ethiopia-Afar Geoscientific Lithospheric Experiment 6TD Passive Array	91	2002–2003
XV	Investigation of Sources of Intraplate Volcanism using PASSCAL Broadband Instruments in Madagascar, the Comores, and Mozambique	34	2011–2013
XW	Broadband seismic experiment in Northeast Uganda to investigate plume-lithosphere interactions	9	2017–2018
XZ	Dhofar Seismic Experiment	11	2003–2004
Y1	Crust and mantle structure and the expression of extension in the Turkana Depression of Kenya and Ethiopia	1	2018–2021
Y6	Rift valley volcanism past present and future	40	2016–2017
YA	Dynamics of the Lake Kivu System	8	2012–2013
YF	Midsea—Mantle Investigation of the Deep Suture between Eurasia and Africa	4	1980–2002

Table 1
Continued

Network code	Network name/description	Number of stations	Operational duration
YH	AfricaArray Southeast Tanzania Basin Experiment	8	2010–2011
YI	2009 Malawi Earthquake RAMP Response	7	2010
YJ	Ethiopia-Afar Geoscientific Lithospheric Experiment	31	2001–2003
YQ	Study of Extension and Magmatism in Malawi and Tanzania	57	2013–2016
YR	Horn of Africa Broadband temporary experiment	3	1999–2002
YR	Dhofar Seismic Experiment II	21	2005–2007
YY	Exploring extensional tectonics beyond the Ethiopian Rift	33	2013–2016
YZ	Boina Broadband Network	9	2005–2007
ZE	AFAR07	19	2007–2009
ZE	SELASOMA Project, Madagascar	49	2012–2014
ZF	Afar Consortium Network	32	2007–2009
ZI	CoMITAC Morocco-Bristol Network	6	2011–2013
ZK	Afar Depression Dense Seismic Array	18	2009–2011
ZP	Africa Array- Uganda/Tanzania	37	2007–2009
ZP	Africa Array- Uganda/Tanzania	35	2010–2013
ZS	Tanzania 2007, Tanzania Broadband temporary experiment	22	2007–2008
ZT	REU: Imaging the Bushveld Complex, South Africa	23	2015–2020
ZU	North Tanzania	3	2008
ZV	Southern Lake Tanganyika experiment	13	2014–2015

Note. Data from these arrays are openly available through the IRIS DMC.

In the above equation, A is the sensitivity matrix (see Kárason & van der Hilst, 2000; Li et al., 2008), m is the velocity model vector, d is the data vector containing the travel-time residual measurements, and L is a smoothing operator. To suppress noise in the data and to prevent the inversion from varying too far from the reference model (and hence being unrealistic), the k_{1-3} terms are included to control the damping and smoothing of the inversion. Further, body waves travel along near-vertical paths in the shallow subsurface, and this may cause crustal anomalies to "smear" downward into the mantle. Therefore, the last term on the right side of Equation 1 regularizes the crustal structure using an *a priori* 3-D crustal model (C), where M_c is the crustal part of the model space. This approach balances the crustal and upper mantle contributions to the misfit (Hansen et al., 2012; Li et al., 2008). For our study, the CRUST1.0 model (Laske et al., 2012) is used for C. While our investigation is focused on the mantle structure beneath Africa, specifically beneath Cameroon, the global inversion accounts for structural heterogeneities outside the region of interest. After 200 iterations, the error function was reduced by 93%, and the misfit vector decreased from 0.95 to 0.25 s, indicating the improvement in data fit between the starting and final models. Figures 3 and 4 show map-view images at selected mantle depths and several cross-sections through our new model, respectively, with an additional cross-section shown in Figure S2 of Supporting Information S1. All images of our new tomographic model are plotted as percent variations in P-wave velocity (δV_p) relative to the reference model (Kennett et al., 1995).

3. Results and Resolution Tests

Similar to many continental- and global-scale tomographic models (e.g., Boyce et al., 2021; Forte et al., 2010; Hansen & Nyblade, 2013; Hansen et al., 2012; Hosseini et al., 2020; Montelli et al., 2004; Tsekhmistrenko et al., 2021; Zhao et al., 2013), our results show slow seismic velocities in the lower mantle (~1,600–2,800 km) beneath southern Africa, which are attributed to the African LLVP, a large-scale, thermo-chemical anomaly that originates near the core-mantle boundary (CMB). Our model also displays anomalously slow velocities at shallow

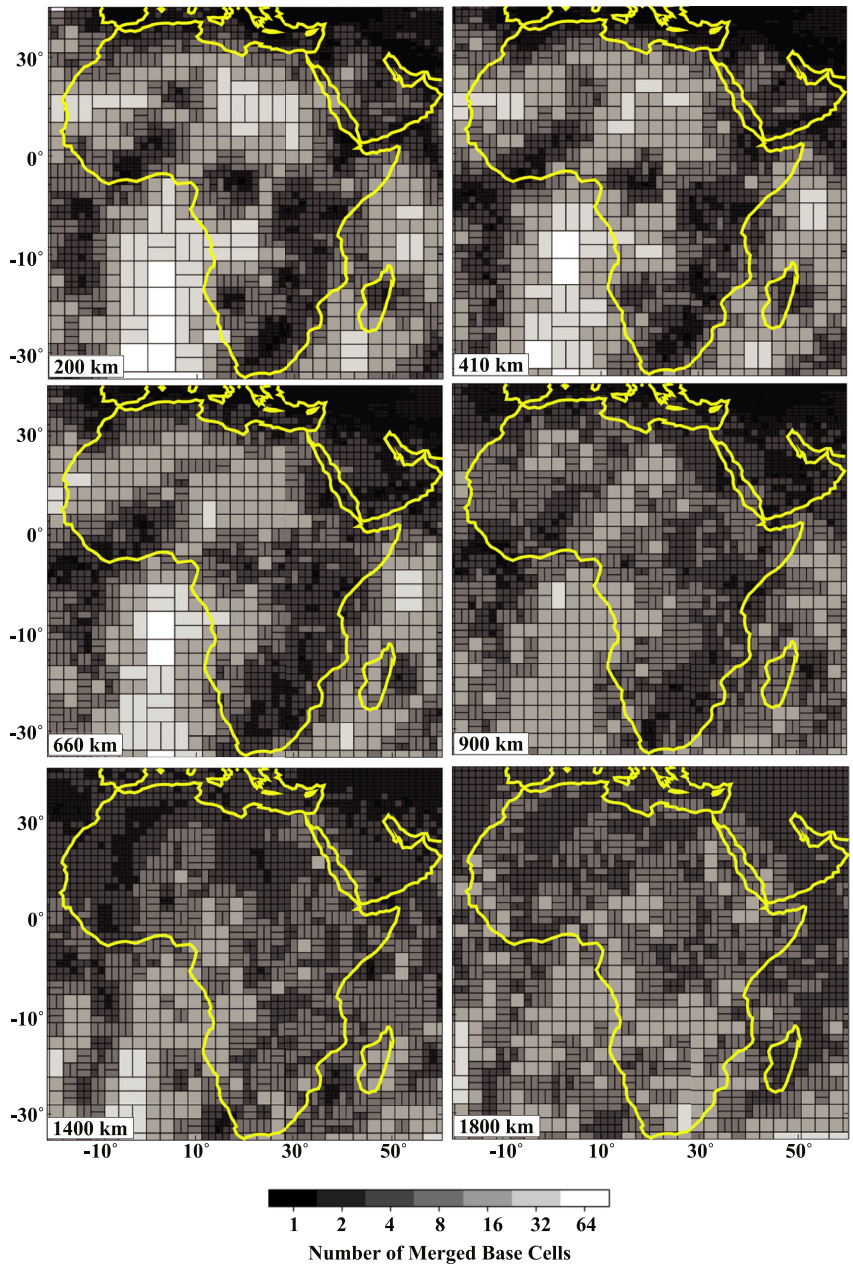

Figure 2. The adaptive grid for our new tomographic model, shown at selected mantle depths. Values on the color scale indicate the number of base cells (0.7° × 0.7°) encompassed by each adaptive grid cell, and the adaptive cells are shaded, with smaller grid cells having darker colors and larger cells having lighter colors. As noted in the text, all adaptive grid cells are required to have a ray count of at least 900; therefore, the darker (smaller) cells are associated with areas of greater raypath coverage and higher resolution. The resolution of our model is better at mid- to lower mantle depths compared to the shallow mantle.

mantle depths (~100–600 km) beneath the CVL as well as fast velocities beneath the West African and Congo Cratons, comparable to previous regional studies (Figures 3 and 4; Figure S2 in Supporting Information S1; Adams et al., 2015; Goussi Ngalamo et al., 2018; Guidarelli & Aoudia, 2016; Reusch et al., 2010). Furthermore, our results strongly suggest that the shallow CVL structure is connected to the African LLVP through the mid- and lower mantle (Figure 4). The deep, slow velocities beneath southern Africa extend northwestward beneath the fast Congo Craton, but at ~10°S latitude, the slow velocities start to shallow and reach the near surface at ~2°N latitude beneath Cameroon. As noted previously, some prior tomographic models (Figure S1 in Supporting Information S1; e.g., Simmons et al., 2010, 2012; Tesoniero et al., 2015) provide some indication of similar

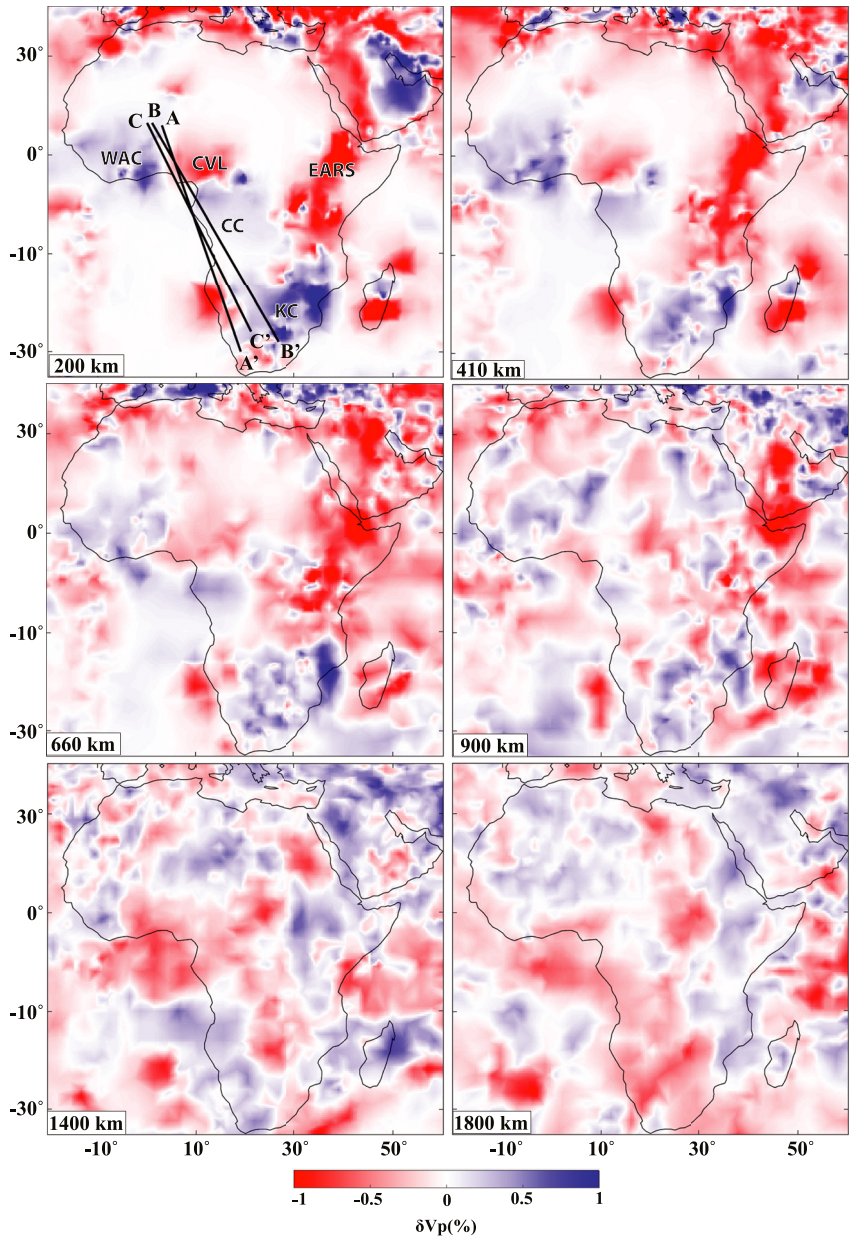

Figure 3. Map-view images of our new P-wave tomography model at selected mantle depths. All panels show the percent variation of P-wave velocity (δV_P) relative to the reference model (Kennett et al., 1995). Black lines labeled A–A′, B–B′, and C–C′ in the 200 km depth panel show the locations of cross-sections in Figure 4. Tectonic features are also labeled. EARS: East African Rift System; KC: Kaapvaal Craton; CC: Congo Craton; CVL: Cameroon Volcanic Line; WAC: West African Craton.

structure; however, these models do not display the CVL-LLVP connection as clearly as our results, and no prior investigation has fully investigated this possibility.

To assess the resolution of our new model and the reliability of the CVL-LLVP connection, we performed two sets of resolution tests. The first are checkerboard tests, implemented as predefined slow and fast anomalies adjacent to one another to form a checkerboard pattern. Input anomalies for the checkerboard tests include 5° × 5° checkers with ±2% velocity perturbations, which have been projected onto the adaptive grid (Figures 2 and 5a; Figure S3 in Supporting Information S1). The checkers are centered at different depths to assess lateral and vertical resolution throughout the model space (Figure 5; Text S3 and S4 in Supporting Information S1). Synthetic travel-times are created and inverted with the same input parameters as those used for the real data, though noise

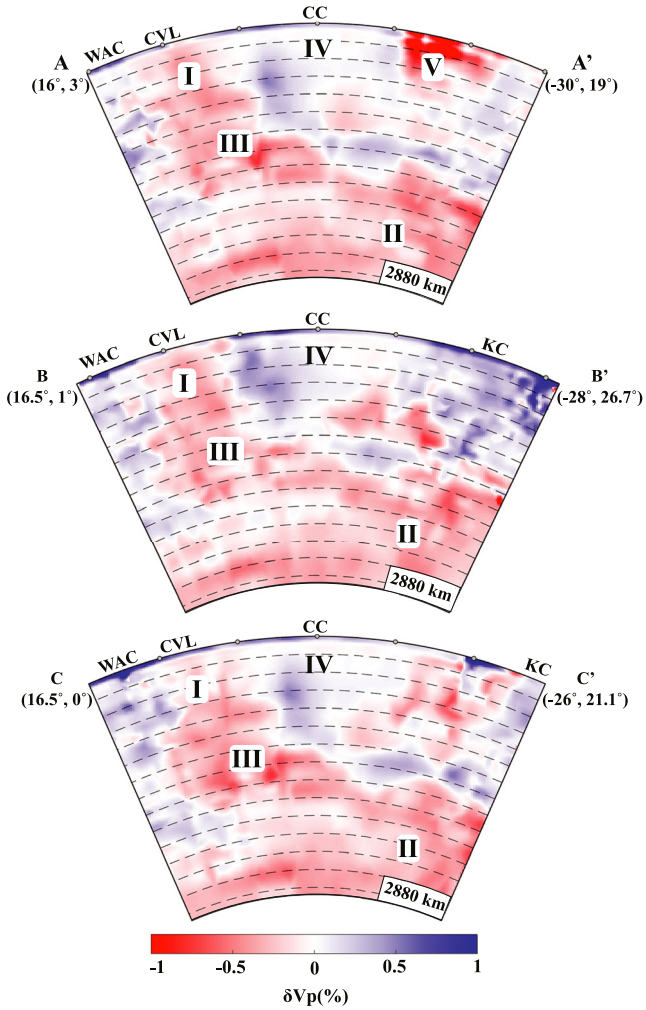

Figure 4. Cross-sectional profiles extending between western and southern Africa, passing through the center of the Cameroon Volcanic Line (CVL) (see Figure 3). Dashed lines mark the depth in 200 km increments. These profiles illustrate that the slow velocities beneath the CVL (I) and those associated with the African Large Low Velocity Province (II) are connected across the mid-mantle (III). The fast, shallow region in the center of each profile (IV) corresponds to the Congo Craton. The shallow, slow region on the southern end of profile A–A′ (V) is located near the coast of Angola, close to Bie Dome (Figure 1a). Fast, upper mantle velocities at the northern ends of each profile are associated with the West African Craton, and those at the southern ends of profiles B–B′ and C–C′ are associated with the Kaapvaal Craton.

is added to the synthetic travel-times as a Gaussian residual time error with a standard deviation of 0.25 s. The error estimate corresponds to the weighted average of the residual remaining in our model after inversion, thereby reproducing the same fit to the synthetic data as that obtained in the actual model (Hansen et al., 2014; Rawlinson et al., 2014). The recovered models between ~200 and 600 km depth (Figures 5b and 5c) demonstrate that the shallow onshore portion of the CVL is fairly well resolved, but resolution of the offshore portion is limited. Amplitude recovery in the upper ~600 km of our model is ~50% in areas with dense seismic station coverage; however, it reduces to ~30% in areas with less data sampling. Given the steep orientation of P-wave ray paths in the shallow mantle, ~200 km of vertical smearing is also observed (see Figure S4 in Supporting Information S1). Between ~600 and 2,000 km depth, amplitude recovery is close to uniform (~50%), though limited areas have ~60% recovery, and vertical smearing is greatly reduced (~100 km; Figures 5d–5f; Figures S3 and S4 in Supporting Information S1).

The second set of resolution tests includes synthetic fast and slow anomalies at specific depths in the mantle to represent features of interest. Specifically, we want to assess if the slow upper mantle beneath the CVL is connected to the slow structure observed at ~1,800 km depth, which extends southeastward toward southern Africa (Figure 4). Two versions of these targeted synthetic tests are shown in Figure 6. In the first, the slow signature beneath the CVL and at depth are represented with synthetic anomalies that are connected across the mid-mantle (Figure 6a, anomalies I–III). Input amplitudes ranging from −1.4% to −1.2% are used to reproduce the observed structure. Another slow anomaly (−3%, Figure 6a, anomaly V) is included at ~20°S latitude to represent the slow velocity structure observed on the southern end of profile A–A′ (Figure 4). Additionally, a fast anomaly (+1%) above 200 km depth (Figure 6a, anomaly IV) is included between ~0° and ~20°S latitude to represent the Congo Craton. As with the checkerboard tests (Figure 5), the synthetic anomalies are projected onto the irregular grid (Figure 2). The second targeted synthetic test is similar to the first, but in this case, the CVL anomaly (Figure 6b, anomaly I) is truncated at 660 km depth and is no longer connected to the deep mantle anomaly (Figure 6b, anomaly II) through the mid mantle. The input amplitudes of the synthetic anomalies range from −1% to −1.2% to mimic the observed amplitudes as close as possible. The recovered models (Figures 6c–6h) show that the fast anomaly associated with the Congo Craton is not well resolved above ~200 km depth and that the anomaly tends to smear vertically downwards. No seismic stations exist in this region of Africa (Figure 1b), so raypath coverage is significantly reduced, and the shallow mantle structure is not well recovered. The slow anomaly at the southern end of profile A–A′ (Figure 6, anomaly V) is better resolved, though its boundaries are not well defined given both vertical and lateral smearing to the northwest (Figures 6c–6h).

That said, both our checkerboard resolution tests (Figure 5; Figures S3 and S4 in Supporting Information S1), and our targeted synthetic tests (Figure 6; Figure S5 in Supporting Information S1) demonstrate that the structure below ~600 km depth is well resolved. This is further illustrated by the denser adaptive gridding in our model (Figure 2) and the extensive raypath coverage in western and southern Africa (Text S3 and Figures S6–S8 in Supporting Information S1), highlighting our robust sampling of structures at critical mid- and lower mantle depths. While some vertical smearing does occur (Figure 6), a discontinuous structure (Figures 6b and 6f–6h) between the CVL and the LLVP does not match our model observations (Figure 4). Instead, our results closely match a continuous low-velocity structure that extends across the mid- and lower mantle (Figures 6a and 6c–6e). We note that a third targeted synthetic test was also performed (Text S2 and Figure S5 in Supporting Information S1) to assess if anomaly III (Figures 4 and 6a) could be associated with off-profile structure that may

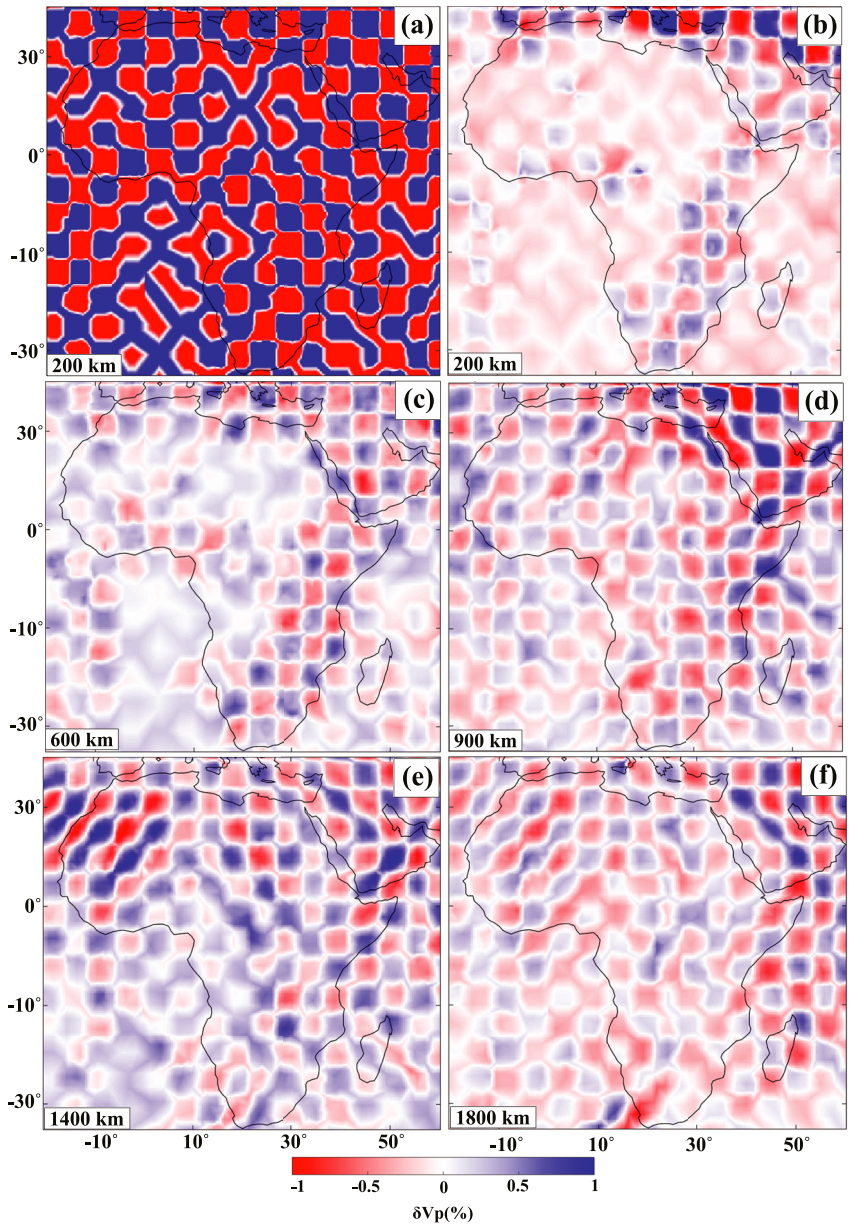

Figure 5. Checkerboard resolution tests. (a) Example 5° × 5° input checkers with ±2% velocity variations, which have been projected onto the irregular grid at 200 km depth. (b) Recovered checkers at 200 km depth. Other panels (c–f) show the recovered checkers for input patterns at the mantle depths indicated. Amplitude recovery generally ranges from ~30% to 60%.

potentially smear into the examined region; however, as shown in Figure S5 of Supporting Information S1, such structure cannot explain our observations.

4. Discussion and Interpretation

4.1. Upper Mantle Convection

Our model results and synthetic tests (Figures 3–6; Supporting Information S1) do not agree well with models that attribute the origin of the CVL only to convective upper mantle flow. Even if the largest convection cell size is considered (Meyers et al., 1998), the anomalously slow material beneath the CVL should be concentrated in the upper ~600–700 km of the mantle and would not continue across the transition zone into the lower mantle (similar to Figure 6b). This line of argument is supported by Reusch et al. (2011), who used their receiver function

10.1029/2022GC010621

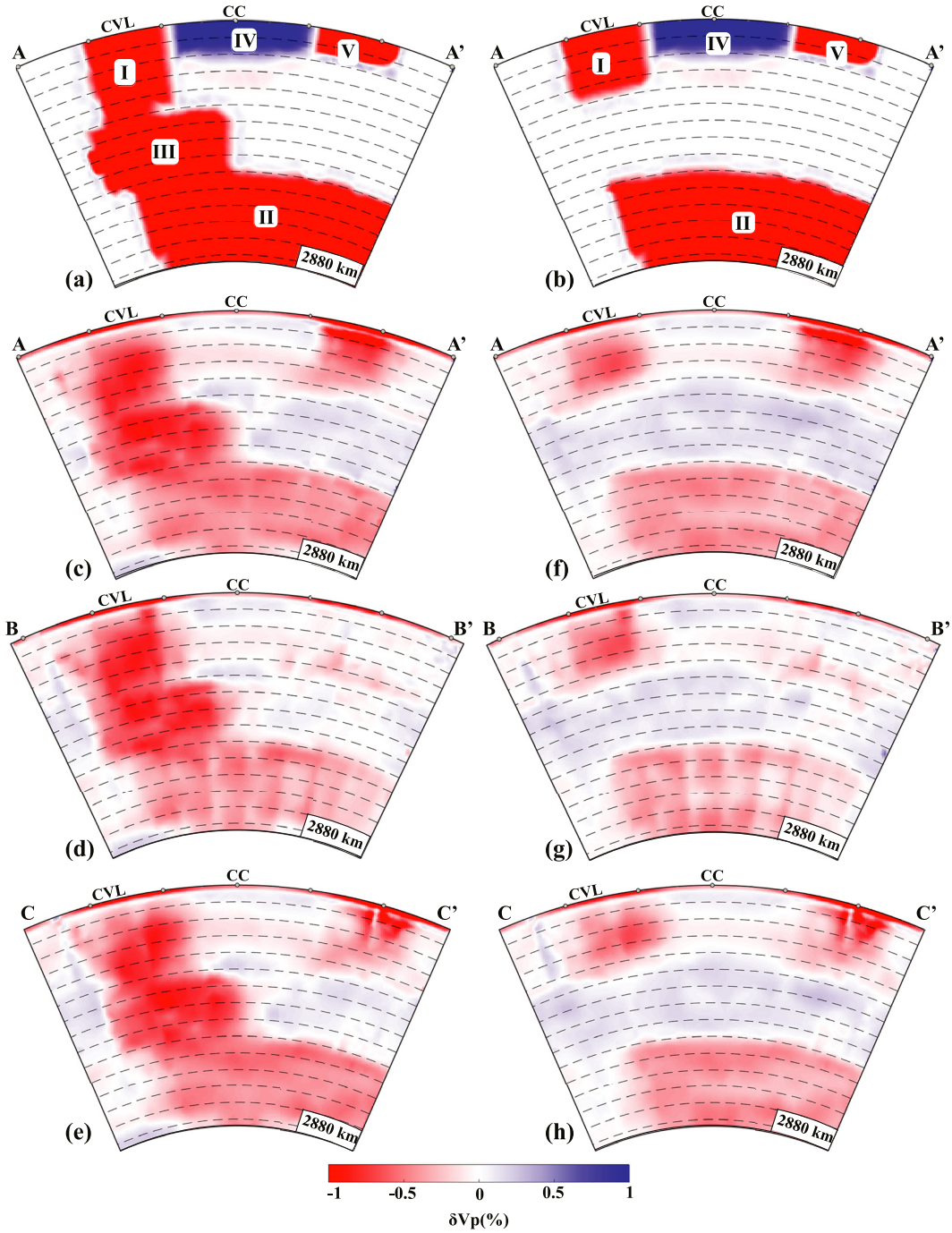

Figure 6. Targeted resolution tests along the same cross-sectional profiles shown in Figure 4. Dashed lines mark the depth in 200 km increments. Panels (a) and (b) show two different input models, with the synthetic anomalies (I–V) corresponding to observed features (Figure 4). The associated recovered models along each examined profile are shown in the lower panels (c–h). Results in the left column (panels c–e), where the shallow Cameroon Volcanic Line anomaly (I) is connected to the African Large Low Velocity Province anomaly (II) across the mid-mantle (III) provide a better match to the observed structure shown in Figure 4. CC: Congo Craton.

results to demonstrate that the mantle transition zone beneath the CVL has a nearly uniform thickness that is similar to the global average, indicating that upper mantle thermal anomalies do not reach these depths.

In contrast, our results provide strong evidence for a connection between the lower mantle African LLVP and the CVL, crossing the mantle transition zone (which is typically between 410 and 660 km depth) at ~3°N latitude

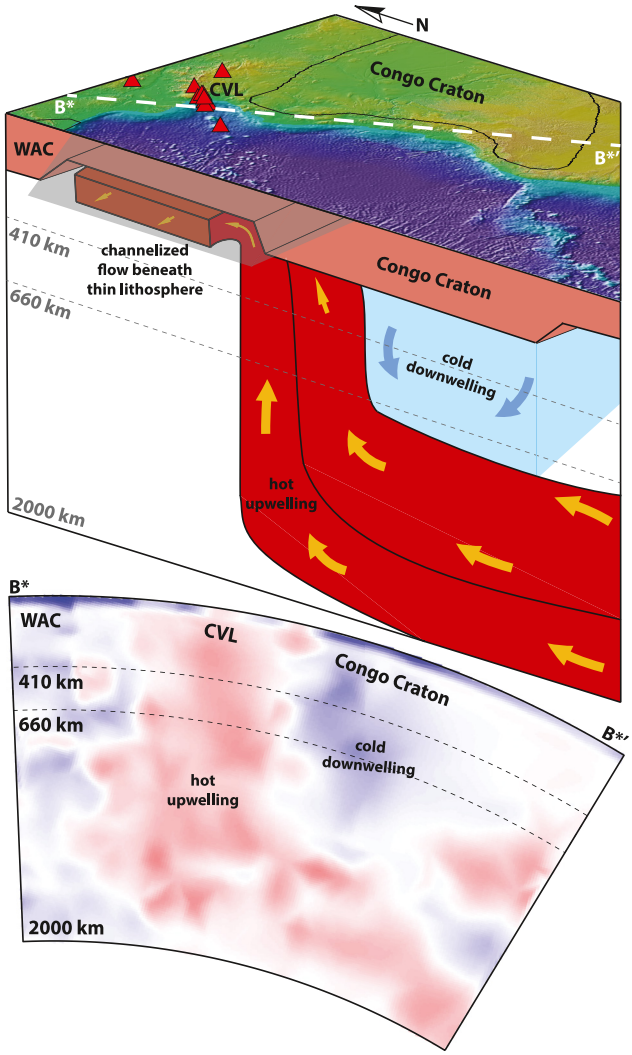

Figure 7. (top) Cartoon illustrating the proposed Cameroon Volcanic Line (CVL) origin mechanism, based on our new tomographic model and on constraints from previous studies (not drawn to scale). White dashed line marks profile B*–B*′, which is a truncated version of profile B-B' (Figure 4). (bottom) Tomography along profile B*–B*′, focused on the structure beneath western Africa. Both panels show slow material (red) generated near the core-mantle boundary at the African Large Low Velocity Province moving northwestward beneath the Congo Craton. This material remains at depth given sublithospheric downwelling (blue) beneath the craton. However, once the northern edge of the craton is reached, the hot material rises toward the surface, ultimately leading to CVL volcanism. Hot mantle material may be laterally channelized along thinner lithosphere beneath the CVL, creating its offshore branch. The thinner CVL lithosphere and channelized flow (gray shaded region in cartoon) is inferred from other studies (e.g., de Plaen et al., 2014; Reusch et al., 2010) since the shallow mantle structure, particularly offshore, is not well resolved in our model (Figure 5). WAC: West African Craton.

(Figure 4). To investigate the potential discrepancy between our findings and those of Reusch et al. (2011), we estimate the mantle transition zone thinning expected from our observed anomaly. Our model indicates a V_P reduction of ~0.4% at transition zone depths (Figures 3 and 4), compared to the AK135 reference model (Kennett et al., 1995). We double this estimate to 0.8% to better account for the true velocity signature given the ~50% amplitude recovery in our model. Using the reference velocity values and the same P-to-S velocity ratio (Kennett et al., 1995), our observed anomaly is estimated to have a S-wave velocity (V_S) signature that is ~0.03 and 0.05 km/s slower than the reference V_S values at the top and bottom of the transition zone, respectively (see Text S4 in Supporting Information S1). Furthermore, using the relationship from Faul and Jackson (2005), we can relate these V_S differences to temperature deviations, which in turn, can be used to estimate the degree of transition zone thinning associated with the observed anomaly. We find that the slow velocity anomaly beneath the CVL would lead to an overall mantle transition zone thinning of ~5 km, which is lower than the Reusch et al. (2011) resolution threshold (±10 km). In other words, the imaged CVL anomaly would only result in minimal transition zone thinning that would not be resolved by the receiver function analysis.

4.2. A Deep Mantle Source for the CVL

Given the strong evidence our results provide for a connection between the African LLVP and the CVL, we suggest the CVL is linked to lower mantle processes. More specifically, we suggest that slow velocity (i.e., hotter and lower density than average) material generated near the CMB beneath southern Africa flows northwestward from the African LLVP and beneath the Congo Craton. At the northern edge of the craton, the hot, buoyant material rises through the mantle, ultimately leading to the volcanism observed in the onshore section of the CVL (Figure 7). Our interpretation is somewhat similar to the mechanism suggested by Forte et al. (2010); however, in their model, the CVL is associated with a large-scale upwelling beneath Cape Verde, which they refer to as the "West African Superplume" and which is interpreted to be a separate mantle anomaly from the widely recognized African LLVP. While both our results and those of Forte et al. (2010) suggest that CVL volcanism is dominantly driven by flow that originates in the deep mantle, the source of this material differs between the studies.

One key question is why the anomalously slow material trending northwestward from southern Africa remains at depth south of ~10°S latitude (Figure 4). Several prior studies (Forte et al., 2010; French & Romanowicz, 2015) have suggested mantle upwellings at the edges of the Congo Craton, like that proposed here to explain the CVL. Geodynamic models (Forte et al., 2010; Moucha & Forte, 2011) indicate that such upwellings would drive sublithospheric downwelling beneath the craton. This convective drawdown may prevent hot, buoyant material at depth from ascending until the material reaches the edges of the convective cell (Figure 7). We also note that small-scale convection, such as that suggested by Reusch et al. (2010, 2011) and Adams et al. (2015; see Section 4.1), could also occur at shallow mantle depths beneath the CVL. However, our findings indicate that this would be secondary flow, superimposed on the larger scale flow field and that it would not be the dominant source of volcanism in the study area.

Other lines of evidence also support the CVL being linked to the African LLVP. For example, geochemical analyses from Jackson et al. (2018), Ziem à Bidias et al. (2018, 2021), and Asaah et al. (2015, 2021) report that

CVL lavas originate from an enriched mantle source with a high-μ signature, thereby providing evidence for a deep mantle contribution. Gravity modeling in western-central Africa is also consistent with our interpreted mechanism. Balogun and Akintokewa (2020), for instance, suggest that trends with wavelengths of 300–500 km in regional-scale gravity data are likely associated with a mantle upwelling, which they attribute to the African LLVP. Marcel et al. (2018) showed positive gravity anomalies beneath Mount Cameroon, resulting from dense material at crustal depths, and they suggested that such anomalies are caused by mantle upwelling from depth.

It is also possible that anomaly V (Figures 4 and 6), which has also been recognized in previous tomographic studies (e.g., Emry et al., 2019; Hansen et al., 2012), may be associated with the same type of mantle structure as that interpreted for the CVL. Just as hot mantle material moves under the Congo Craton and emerges along its northern edge, thereby forming the CVL, the same anomalous material may seep outward along the southwestern edge of the craton to generate this anomalous feature. We note that anomaly V is located just south of Bie Dome (Figure 1a), an uplifted region that several studies have associated with dynamic topography due to mantle upwelling (Al-Hajri et al., 2009; Giuliani et al., 2017; Walker et al., 2016). That said, given the generally low resolution of our model at shallow mantle depths, coupled with the extent of vertical smearing in this region, it is difficult to assess the potential connection between anomaly V, Bie Dome, and the broad-scale anomaly we observe at depth.

4.3. The Offshore Component of the CVL

The offshore portion of the CVL is difficult to assess given the limited upper mantle resolution of our model in this region (Figure 5). However, comparing our results to those of prior investigations, we can speculate on how the offshore portion of the volcanic line may have developed. While the onshore segment of the CVL does not display any evidence for volcanic age progression, there is some indication of age progression in the offshore segment, with ages possibly decreasing from Príncipe Island to São Tomé and Annobón further to the southwest (Figure 1a; e.g., Cornen & Maury, 1980; Dunlop & Fitter, 1979; Grunau et al., 1975; Lee et al., 1994). Reusch et al. (2010) suggested that warm mantle material under the continental portion of the CVL may be channeled offshore by topography on the underside of the lithosphere related to fracture zones (Figure 7), and they remarked that this could potentially explain the offshore age trend. Alternatively, the oceanic CVL lithosphere may have been thinned by small-scale delamination resulting from instabilities that could have developed at the edge of the continent, as demonstrated by the laboratory experiments from Milelli et al. (2012), thereby creating topography that directs shallow sublithospheric mantle flow offshore. Seismic anisotropy measurements also support this suggestion (de Plaen et al., 2014; Elsheikh et al., 2014; Koch et al., 2012). Further, geochemical analyses (Rankenburg et al., 2005) indicate that some lavas from the oceanic portion of the CVL display a continental crustal component that could be caused by shallow contamination. Thus, sublithospheric topography could direct some hot mantle material originating at depth, as interpreted from our results, beneath the offshore branch of the CVL (Figure 7).

5. Conclusions

We have developed a new P-wave velocity model for Africa using an extensive travel-time residual data set and an adaptively parameterized tomographic approach. Our results provide high resolution imaging of the mid- and lower mantle structure beneath western Africa, which we employ to further assess origin models for the CVL. The new model and associated resolution tests provide strong evidence for a connection between the African LLVP and the CVL. We suggest that low velocity material generated in the lower mantle beneath southern Africa moves northwestward beneath the Congo Craton. At the northern edge of the craton, the hot, buoyant material rises through the mantle, ultimately leading to the observed onshore volcanism. The hot mantle material may also be laterally channelized along thinner lithosphere beneath the CVL, creating the offshore branch of the system. Ultimately, our results illustrate that deep, lower mantle processes may significantly impact Earth surface processes, such as the formation of volcanic provinces.

Data Availability Statement

Data management handling was provided by the Incorporated Research Institutions for Seismology Data Management Center (IRIS DMC; http://ds.iris.edu/mda/), which is funded through the Seismological Facilities for the Advancement of Geoscience award of the NSF under cooperative support agreement EAR-1851048. Some figures were generated with Generic Mapping Tools (Wessel et al., 2013).

Acknowledgments
We thank Scott King and an anonymous reviewer for their thorough critiques of our manuscript. Much of the new seismic data used in this study were collected by projects supported by the National Science Foundation (Grants 0440032, 0530062, 0824781, 1128936, and 1634108).

References

Adams, A. N. (2022). Insights into the source of magmatic hot-lines: Forty years of geophysical studies of the Cameroon Volcanic Line. *Frontiers in Earth Science*, *10*, 1–20. https://doi.org/10.3389/feart.2022.838993

Adams, A. N., Wiens, D. A., Nyblade, A. A., Euler, G. G., Shore, P. J., & Tibi, R. (2015). Lithospheric instability and the source of the Cameroon Volcanic Line: Evidence from Rayleigh wave phase velocity tomography. *Journal of Geophysical Research: Solid Earth*, *120*(3), 1708–1727. https://doi.org/10.1002/2014JB011580

Al-Hajri, Y., White, N., & Fishwick, S. (2009). Scales of transient convective support beneath Africa. *Geology*, *37*(10), 883–886. https://doi.org/10.1130/G25703A.1

Asaah, A. N. E., Yokoyama, T., Aka, F. T., Usui, T., Wirmvem, M. J., Chako Tchamabe, B., et al. (2015). A comparative review of petrogenetic processes beneath the Cameroon Volcanic Line: Geochemical constraints. *Geoscience Frontiers*, *6*(4), 557–570. https://doi.org/10.1016/j.gsf.2014.04.012

Asaah, A. N. E., Yokoyama, T., Iwamori, H., Aka, F. T., Kuritani, T., Usui, T., et al. (2021). High–μ signature in lavas of Mt. Oku: Implications for lithospheric and asthenospheric contributions to the magmatism of the Cameroon Volcanic Line (West Africa). *Lithos*, *400–401*, 106416. https://doi.org/10.1016/j.lithos.2021.106416

Balogun, O. B., & Akintokewa, O. C. (2020). Analysis and interpretation of regional-scaled gravity measurements in the central equatorial Atlantic region of Africa. *Rudarsko-Geolosko-Naftni Zbornik*, *35*(1), 81–99. https://doi.org/10.17794/rgn.2020.1.7

Bastow, I. D., Nyblade, A. A., Stuart, G. W., Rooney, T. O., & Benoit, M. H. (2008). Upper mantle seismic structure beneath the Ethiopian hot spot: Rifting at the edge of the African low-velocity anomaly. *Geochemistry, Geophysics, Geosystems*, *9*(12), Q12022. https://doi.org/10.1029/2008GC002107

Bonneville, A., Dosso, L., & Hildenbrand, A. (2006). Temporal evolution and geochemical variability of the South Pacific superplume activity. *Earth and Planetary Science Letters*, *244*(1–2), 251–269. https://doi.org/10.1016/j.epsl.2005.12.037

Boyce, A., Bastow, I. D., Cottaar, S., Kounoudis, R., Guilloud De Courbeville, J., Caunt, E., & Desai, S. (2021). AFRP20: New P-wavespeed model for the African mantle reveals two whole-mantle plumes below East Africa and Neoproterozoic modification of the Tanzania craton. *Geochemistry, Geophysics, Geosystems*, *22*(3), e2020GC009302. https://doi.org/10.1029/2020GC009302

Boyce, A., Bastow, I. D., Rondenay, S., & van der Hilst, R. D. (2017). From relative to absolute teleseismic travel times: The Absolute Arrival-time Recovery Method (AARM). *Bulletin of the Seismological Society of America*, *107*(5), 2511–2520. https://doi.org/10.1785/0120170021

Burke, K. (2001). Origin of the Cameroon line of volcano-capped swells. *The Journal of Geology*, *109*(3), 349–362. https://doi.org/10.1086/319977

Cornen, G., & Maury, R. C. (1980). Petrology of the volcanic island of Annobon, Gulf of Guinea. *Marine Geology*, *36*(3–4), 253–267. https://doi.org/10.1016/0025-3227(80)90090-0

de Plaen, R. S. M., Bastow, I. D., Chambers, E. L., Keir, D., Gallacher, R. J., & Keane, J. (2014). The development of magmatism along the Cameroon Volcanic Line: Evidence from seismicity and seismic anisotropy. *Journal of Geophysical Research: Solid Earth*, *119*(5), 4233–4252. https://doi.org/10.1002/2013JB010583

Déruelle, B., Moreau, C., Nkoumbou, C., Kambou, R., Lissom, J., Njonfang, E., et al. (1991). The Cameroon line: A review. In *Magmatism in extensional structural settings* (pp. 274–327). Springer Berlin Heidelberg. https://doi.org/10.1007/978-3-642-73966-8_12

Dunlop, H. M., & Fitter, J. G. (1979). A K-Ar and Sr-isotopic study of the volcanic rocks of the island of Príncipe, West Africa—Evidence for mantle heterogeneity beneath the Gulf of Guinea. *Contributions to Mineralogy and Petrology*, *71*(2), 125–131. https://doi.org/10.1007/BF00375428

Ebinger, C. J., & Sleep, N. H. (1998). Cenozoic magmatism throughout east Africa resulting from impact of a single plume. *Nature*, *395*(6704), 788–791. https://doi.org/10.1038/27417

Elsheikh, A. A., Gao, S. S., & Liu, K. H. (2014). Formation of the Cameroon Volcanic Line by lithospheric basal erosion: Insight from mantle seismic anisotropy. *Journal of African Earth Sciences*, *100*, 96–108. https://doi.org/10.1016/j.jafrearsci.2014.06.011

Emry, E. L., Shen, Y., Nyblade, A. A., Flinders, A., & Bao, X. (2019). Upper mantle Earth structure in Africa from full-wave ambient noise tomography. *Geochemistry, Geophysics, Geosystems*, *20*(1), 120–147. https://doi.org/10.1029/2018GC007804

Engdahl, E. R., van der Hilst, R., & Buland, R. (1998). Global teleseismic earthquake relocation with improved travel times and procedures for depth determination. *Bulletin of the Seismological Society of America*, *88*(3), 722–743.

Faul, U., & Jackson, I. (2005). The seismological signature of temperature and grain size variations in the upper mantle. *Earth and Planetary Science Letters*, *234*(1–2), 119–134. https://doi.org/10.1016/j.epsl.2005.02.008

Fitton, J. G., & Dunlop, H. M. (1985). The Cameroon line, West Africa, and its bearing on the origin of oceanic and continental alkali basalt. *Earth and Planetary Science Letters*, *72*(1), 23–38. https://doi.org/10.1016/0012-821X(85)90114-1

Forte, A. M., Quéré, S., Moucha, R., Simmons, N. A., Grand, S. P., Mitrovica, J. X., & Rowley, D. B. (2010). Joint seismic-geodynamic-mineral physical modelling of African geodynamics: A reconciliation of deep-mantle convection with surface geophysical constraints. *Earth and Planetary Science Letters*, *295*(3–4), 329–341. https://doi.org/10.1016/j.epsl.2010.03.017

French, S. W., & Romanowicz, B. A. (2014). Whole-mantle radially anisotropic shear velocity structure from spectral-element waveform tomography. *Geophysical Journal International*, *199*(3), 1303–1327. https://doi.org/10.1093/gji/ggu334

French, S. W., & Romanowicz, B. A. (2015). Broad plumes rooted at the base of the Earth's mantle beneath major hotspots. *Nature*, *525*(7567), 95–99. https://doi.org/10.1038/nature14876

Giuliani, A., Campeny, M., Kamenetsky, V. S., Afonso, J. C., Maas, R., Melgarejo, J. C., et al. (2017). Southwestern Africa on the burner: Pleistocene carbonatite volcanism linked to deep mantle upwelling in Angola. *Geology*, *45*(11), 971–974. https://doi.org/10.1130/G39344.1

Goussi Ngalamo, J. F., Sobh, M., Bisso, D., Abdelsalam, M. G., Atekwana, E., & Ekodeck, G. E. (2018). Lithospheric structure beneath the Central Africa Orogenic Belt in Cameroon from the analysis of satellite gravity and passive seismic data. *Tectonophysics*, *745*, 326–337. https://doi.org/10.1016/j.tecto.2018.08.015

Grunau, H. R., Lehner, P., Cleintuar, M. R., Allenbach, P., & Bakker, G. (1975). New radiometric ages and seismic data from Fuerteventura (Canary Islands), Maio (Cape Verde Islands), and Sao Tome (Gulf of Guinea). In G. J. Borradaile (Ed.), *Progress in Geodynamics: Proceedings of the National Symposium on Geodynamics* (pp. 90–118). North-Holland. Retrieved from http://inis.iaea.org/Search/search.aspx?orig_q=RN:6214998

Guidarelli, M., & Aoudia, A. (2016). Ambient noise tomography of the Cameroon Volcanic Line and Northern Congo craton: New constraints on the structure of the lithosphere. *Geophysical Journal International*, *204*(3), 1756–1765. https://doi.org/10.1093/gji/ggv561

Halliday, A. N., Dickin, A. P., Fallick, A. E., & Fitton, J. G. (1988). Mantle dynamics: A Nd, Sr, Pb and O isotopic study of the Cameroon line volcanic chain. *Journal of Petrology*, *29*(1), 181–211. https://doi.org/10.1093/petrology/29.1.181

Hansen, S. E., Carson, S. E., Garnero, E. J., Rost, S., & Yu, S. (2020). Investigating ultra-low velocity zones in the southern hemisphere using an Antarctic dataset. *Earth and Planetary Science Letters*, *536*, 116142. https://doi.org/10.1016/j.epsl.2020.116142

Hansen, S. E., Graw, J. H., Kenyon, L. M., Nyblade, A. A., Wiens, D. A., Aster, R. C., et al. (2014). Imaging the Antarctic mantle using adaptively parameterized P-wave tomography: Evidence for heterogeneous structure beneath West Antarctica. *Earth and Planetary Science Letters*, *408*, 66–78. https://doi.org/10.1016/j.epsl.2014.09.043

Hansen, S. E., & Nyblade, A. A. (2013). The deep seismic structure of the Ethiopia/Afar hotspot and the African superplume. *Geophysical Journal International*, *194*(1), 118–124. https://doi.org/10.1093/gji/ggt116

Hansen, S. E., Nyblade, A. A., & Benoit, M. H. (2012). Mantle structure beneath Africa and Arabia from adaptively parameterized P-wave tomography: Implications for the origin of Cenozoic Afro-Arabian tectonism. *Earth and Planetary Science Letters*, *319–320*, 23–34. https://doi.org/10.1016/j.epsl.2011.12.023

Hosseini, K., Sigloch, K., Tsekhmistrenko, M., Zaheri, A., Nissen-Meyer, T., & Igel, H. (2020). Global mantle structure from multifrequency tomography using P, PP and P-diffracted waves. *Geophysical Journal International*, *220*(1), 96–141. https://doi.org/10.1093/gji/ggz394

Jackson, M. G., Becker, T. W., & Konter, J. G. (2018). Evidence for a deep mantle source for EM and HIMU domains from integrated geochemical and geophysical constraints. *Earth and Planetary Science Letters*, *484*, 154–167. https://doi.org/10.1016/j.epsl.2017.11.052

Kárason, H., & van der Hilst, R. D. (2000). Constraints on mantle convection from seismic tomography. *Geophysical Monograph Series*, *121*, 257–276. https://doi.org/10.1029/GM121p0277

Kennett, B. L. N., Engdahl, E. R., & Buland, R. (1995). Constraints on seismic velocities in the Earth from traveltimes. *Geophysical Journal International*, *122*(1), 108–124. https://doi.org/10.1111/j.1365-246X.1995.tb03540.x

King, S. D. (2007). Hotspots and edge-driven convection. *Geology*, *35*(3), 223. https://doi.org/10.1130/G23291A.1

King, S. D., & Ritsema, J. (2000). African hot spot volcanism: Small-scale convection in the upper mantle beneath cratons. *Science*, *290*(5494), 1137–1140. https://doi.org/10.1126/science.290.5494.1137

Koch, F. W., Wiens, D. A., Nyblade, A. A., Shore, P. J., Tibi, R., Ateba, B., et al. (2012). Upper-mantle anisotropy beneath the Cameroon Volcanic Line and Congo Craton from shear wave splitting measurements. *Geophysical Journal International*, *190*(1), 75–86. https://doi.org/10.1111/j.1365-246X.2012.05497.x

Koppers, A. A. P., Staudigel, H., Pringle, M. S., & Wijbrans, J. R. (2003). Short-lived and discontinuous intraplate volcanism in the South Pacific: Hot spots or extensional volcanism? *Geochemistry, Geophysics, Geosystems*, *4*(10), 1089. https://doi.org/10.1029/2003GC000533

Laske, G., Masters, G., Ma, Z., & Pasyanos, M. E. (2012). CRUST1.0: An updated global model of Earth's crust. *European Geophysical Union General Assembly*, *14*, 3743.

Lee, D.-C., Halliday, A. N., Fitton, J. G., & Poli, G. (1994). Isotopic variations with distance and time in the volcanic islands of the Cameroon line: Evidence for a mantle plume origin. *Earth and Planetary Science Letters*, *123*(1–3), 119–138. https://doi.org/10.1016/0012-821X(94)90262-3

Li, C., van der Hilst, R. D., Engdahl, E. R., & Burdick, S. (2008). A new global model for P wave speed variations in Earth's mantle. *Geochemistry, Geophysics, Geosystems*, *9*(5), Q05018. https://doi.org/10.1029/2007GC001806

Marcel, J., Abate Essi, J. M., Meli'i, J. L., Njandjock Nouck, P., Mahamat, A., & Manguelle-Dicoum, E. (2018). Geodynamic insights of the Cameroon Volcanic Line (Western Africa) from isostatic gravity anomalies. *Journal of Geodynamics*, *121*, 36–48. https://doi.org/10.1016/j.jog.2018.07.002

McNutt, M. K., Caress, D. W., Reynolds, J., Jordahl, K. A., & Duncan, R. A. (1997). Failure of plume theory to explain midplate volcanism in the southern Austral islands. *Nature*, *389*(6650), 479–482. https://doi.org/10.1038/39013

Meyers, J. B., Rosendahl, B. R., Harrison, C. G. A., & Ding, Z. D. (1998). Deep-imaging seismic and gravity results from the offshore Cameroon Volcanic Line, and speculation of African hotlines. *Tectonophysics*, *284*(1–2), 31–63. https://doi.org/10.1016/S0040-1951(97)00173-X

Milelli, L., Fourel, L., & Jaupart, C. (2012). A lithospheric instability origin for the Cameroon Volcanic Line. *Earth and Planetary Science Letters*, *335–336*, 80–87. https://doi.org/10.1016/j.epsl.2012.04.028

Montelli, R., Nolet, G., Masters, G., Dahlen, F. A., & Hung, S. H. (2004). Global P and PP traveltime tomography: Rays versus waves. *Geophysical Journal International*, *158*(2), 637–654. https://doi.org/10.1111/j.1365-246X.2004.02346.x

Moreau, C., Regnoult, J. M., Déruelle, B., & Robineau, B. (1987). A new tectonic model for the Cameroon Line, Central Africa. *Tectonophysics*, *141*(4), 317–334. https://doi.org/10.1016/0040-1951(87)90206-X

Morgan, W. J. (1981). Hotspot tracks and the opening of the Atlantic and Indian Oceans. *The Sea*, *7*, 443–487.

Moucha, R., & Forte, A. M. (2011). Changes in African topography driven by mantle convection. *Nature Geoscience*, *4*(10), 707–712. https://doi.org/10.1038/ngeo1235

Nolet, G. (1985). Solving or resolving inadequate and noisy tomographic systems. *Journal of Computational Physics*, *61*(3), 463–482. https://doi.org/10.1016/0021-9991(85)90075-0

Paige, C. C., & Saunders, M. A. (1982). Algorithm 583: LSQR: Sparse linear equations and least squares problems. *ACM Transactions on Mathematical Software*, *8*(2), 195–209. https://doi.org/10.1145/355993.356000

Pavlis, G. L., & Vernon, F. L. (2010). Array processing of teleseismic body waves with the USArray. *Computers & Geosciences*, *36*(7), 910–920. https://doi.org/10.1016/j.cageo.2009.10.008

Poudjom Djomani, Y. H., Diament, M., & Wilson, M. (1997). Lithospheric structure across the Adamawa plateau (Cameroon) from gravity studies. *Tectonophysics*, *273*(3–4), 317–327. https://doi.org/10.1016/S0040-1951(96)00280-6

Rankenburg, K., Lassiter, J. C., & Brey, G. (2005). The role of continental crust and lithospheric mantle in the genesis of Cameroon Volcanic Line lavas: Constraints from isotopic variations in lavas and megacrysts from the Biu and Jos Plateaux. *Journal of Petrology*, *46*(1), 169–190. https://doi.org/10.1093/petrology/egh067

Rawlinson, N., Fichtner, A., Sambridge, M., & Young, M. K. (2014). Seismic tomography and the assessment of uncertainty. *Advances in Geophysics*, *55*, 1–76. https://doi.org/10.1016/BS.AGPH.2014.08.001

Reusch, A. M., Nyblade, A. A., Tibi, R., Wiens, D. A., Shore, P. J., Bekoa, A., et al. (2011). Mantle transition zone thickness beneath Cameroon: Evidence for an upper mantle origin for the Cameroon Volcanic Line. *Geophysical Journal International*, *187*(3), 1146–1150. https://doi.org/10.1111/j.1365-246X.2011.05239.x

Reusch, A. M., Nyblade, A. A., Wiens, D. A., Shore, P. J., Ateba, B., Tabod, C. T., & Nnange, J. M. (2010). Upper mantle structure beneath Cameroon from body wave tomography and the origin of the Cameroon Volcanic Line. *Geochemistry, Geophysics, Geosystems*, *11*(10), Q10W07. https://doi.org/10.1029/2010GC003200

Sandwell, D. T., Winterer, E. L., Mammerickx, J., Duncan, R. A., Lynch, M. A., Levitt, D. A., & Johnson, C. L. (1995). Evidence for diffuse extension of the Pacific Plate from Pukapuka ridges and cross-grain gravity lineations. *Journal of Geophysical Research*, *100*(B8), 15087–15099. https://doi.org/10.1029/95JB00156

Simmons, N. A., Forte, A. M., Boschi, L., & Grand, S. P. (2010). GyPSuM: A joint tomographic model of mantle density and seismic wave speeds. *Journal of Geophysical Research*, *115*(B12), B12310. https://doi.org/10.1029/2010JB007631

Simmons, N. A., Myers, S. C., Johannesson, G., & Matzel, E. (2012). LLNL-G3Dv3: Global P wave tomography model for improved regional and teleseismic travel time prediction. *Journal of Geophysical Research*, *117*(B10), B10302. https://doi.org/10.1029/2012JB009525

Smithsonian Institution. (2013). Global volcanism program. Retrieved from https://volcano.si.edu/

Suh, C. E., Ayonghe, S. N., Sparks, R. S. J., Annen, C., Fitton, J. G., Nana, R., & Luckman, A. (2003). The 1999 and 2000 eruptions of Mount Cameroon: Eruption behaviour and petrochemistry of lava. *Bulletin of Volcanology*, *65*(4), 267–281. https://doi.org/10.1007/S00445-002-0257-7

Tesoniero, A., Auer, L., Boschi, L., & Cammarano, F. (2015). Hydration of marginal basins and compositional variations within the continental lithospheric mantle inferred from a new global model of shear and compressional velocity. *Journal of Geophysical Research: Solid Earth*, *120*(11), 7789–7813. https://doi.org/10.1002/2015JB012026

Tsekhmistrenko, M., Sigloch, K., Hosseini, K., & Barruol, G. (2021). A tree of Indo-African mantle plumes imaged by seismic tomography. *Nature Geoscience*, *14*(8), 612–619. https://doi.org/10.1038/s41561-021-00762-9

Walker, R. T., Telfer, M., Kahle, R. L., Dee, M. W., Kahle, B., Schwenninger, J. L., et al. (2016). Rapid mantle-driven uplift along the Angolan margin in the late Quaternary. *Nature Geoscience*, *9*(12), 909–914. https://doi.org/10.1038/ngeo2835

Wessel, P., Smith, W. H. F., Scharroo, R., Luis, J., & Wobbe, F. (2013). Generic mapping tools: Improved version released. *Eos, Transactions American Geophysical Union*, *94*(45), 409–410. https://doi.org/10.1002/2013EO450001

Weston, J., Engdahl, E. R., Harris, J., di Giacomo, D., & Storchak, D. A. (2018). ISC-EHB: Reconstruction of a robust earthquake data set. *Geophysical Journal International*, *214*(1), 474–484. https://doi.org/10.1093/gji/ggy155

Zhao, D., Yamamoto, Y., & Yanada, T. (2013). Global mantle heterogeneity and its influence on teleseismic regional tomography. *Gondwana Research*, *23*(2), 595–616. https://doi.org/10.1016/j.gr.2012.08.004

Ziem à Bidias, L. A., Chauhan, H., Mekala, R. M., & Rao, N. V. C. (2021). Green core clinopyroxenes from basanites of Petpenoun volcanoes, Noun Plain, Cameroon volcanic line: Chemistry and genesis. *Bulletin of Volcanology*, *83*(3), 13. https://doi.org/10.1007/s00445-021-01437-4

Ziem à Bidias, L. A., Chazot, G., Moundi, A., & Nonnotte, P. (2018). Extreme source heterogeneity and complex contamination patterns along the Cameroon Volcanic Line: New geochemical data from the Bamoun plateau. *Comptes Rendus Geoscience*, *350*(3), 100–109. https://doi.org/10.1016/j.crte.2017.11.004

References From the Supporting Information

Hansen, S. E., Garnero, E. J., & Rost, S. (2021). Historical interstation pattern referencing (HIPR): An application to PcP waves recorded in the Antarctic for ULVZ imaging. *Journal of Geophysical Research: Solid Earth*, *126*(10), e2021JB022741. https://doi.org/10.1029/2021JB022741

Hosseini, K., Matthews, K. J., Sigloch, K., Shephard, G. E., Domeier, M., & Tsekhmistrenko, M. (2018). SubMachine: Web-based tools for exploring seismic tomography and other models of Earth's deep interior. *Geochemistry, Geophysics, Geosystems*, *19*(5), 1464–1483. https://doi.org/10.1029/2018GC007431

Lu, C., Grand, S. P., Lai, H., & Garnero, E. J. (2019). TX2019slab: A new P and S tomography model incorporating subducting slabs. *Journal of Geophysical Research: Solid Earth*, *124*(11), 11549–11567. https://doi.org/10.1029/2019JB017448

Turcotte, D. L., & Schubert, G. (2002). *Geodynamics*. Cambridge University Press. https://doi.org/10.1017/CBO9780511807442